Spherical aggregates of β-amyloid (amylospheroid) show high neurotoxicity and activate tau protein kinase I/glycogen synthase kinase-3β

Minako Hoshi*†‡, Michio Sato*, Shinichiro Matsumoto§, Akihiko Noguchi†, Kaori Yasutake*, Natsuko Yoshida*, and Kazuki Sato*¶

*Mitsubishi Kagaku Institute of Life Sciences, 11 Minamiooya, Machida, Tokyo 194-8511, Japan; †PRESTO, Japan Science and Technology Corp., and §CACs, Inc., 1000 Kamoshida, Aobaku, Yokohama 227-0033, Japan

Edited by Christopher T. Walsh, Harvard Medical School, Boston, MA, and approved April 16, 2003 (received for review November 21, 2002)

β-Amyloid (Aβ) acquires toxicity by self-aggregation. To identify and characterize the toxic form(s) of Aβ aggregates, we examined *in vitro* aggregation conditions by using large quantities of homogenous, chemically synthesized $Aβ_{1–40}$ peptide. We found that slow rotation of $Aβ_{1–40}$ solution reproducibly gave self-aggregated $Aβ_{1–40}$ containing a stable and highly toxic moiety. Examination of the aggregates purified by glycerol-gradient centrifugation by atomic force microscopy and transmission electron microscopy revealed that the toxic moiety is a perfect sphere, which we call amylospheroid (ASPD). Other $Aβ_{1–40}$ aggregates, including fibrils, were nontoxic. Correlation studies between toxicity and sphere size indicate that 10- to 15-nm ASPD was highly toxic, whereas ASPD <10 nm was nontoxic. A positive correlation between the toxicity and ASPD >10 nm also appeared to exist when $Aβ_{1–42}$ formed ASPD by slow rotation. However, $Aβ_{1–42}$-ASPD formed more rapidly, killed neurons at lower concentrations, and showed ≈100-fold-higher toxicity than $Aβ_{1–40}$-ASPD. The toxic ASPD was associated with SDS-resistant oligomeric bands in immunoblotting, which were absent in nontoxic ASPD. Because the formation of ASPD was not disturbed by pentapeptides that break β-sheet interactions, Aβ may form ASPD through a pathway that is at least partly distinct from that of fibril formation. Inhibition experiments with lithium suggest the involvement of tau protein kinase I/glycogen synthase kinase-3β in the early stages of ASPD-induced neurodegeneration. Here we describe the identification and characterization of ASPD and discuss its possible role in the neurodegeneration in Alzheimer's disease.

A 40- to 42-residue peptide named β-amyloid (Aβ) is a major constituent of senile plaques in Alzheimer's disease (AD) (1). Although multiple pathways have been suggested to lead to AD, recent advances indicate a causal link between Aβ and AD (2), and this idea is supported further by findings that vaccination against Aβ ameliorates behavioral deficits in transgenic mice (3–5). Among various *in vivo* Aβ species, $Aβ_{1–42}$ generally is considered as the primary vehicle of toxicity, whereas $Aβ_{1–40}$, a major species under physiological conditions, is considered less harmful and more resistant to the formation of oligomers than $Aβ_{1–42}$ (6). However, it remains controversial which Aβ species contributes predominantly to AD pathogenesis, because both *in vitro* and *in vivo* studies have confirmed toxicity of $Aβ_{1–40}$ aggregates (7, 8).

It has been widely accepted that toxicity of Aβ requires aggregation of native Aβ monomers (9–11). Besides fibrils, several types of nonfibrillar aggregates have been reported: $Aβ_{1–40}$ oligomers from dimers–hexamers (6, 12–14); a mixture of $Aβ_{1–42}$ oligomers named Aβ-derived diffusible ligands (ADDLs), ranging from trimers–hexamers up to 24-mers (15); and fibril intermediates named protofibrils (PFs) (16, 17). All of these aggregates are mixtures of Aβ oligomers with a variety in oligomer size, and precise morphological analysis of each Aβ aggregate is difficult. In other words, the heterogeneity of Aβ aggregates in terms of Aβ species and oligomer size makes it difficult to reach a consensus about the oligomerization state of Aβ causing the pathogenicity. It is yet to be determined whether all of these *in vitro* oligomers actually exist *in vivo* and induce neuronal damage, or whether a particular oligomer is primarily responsible for AD.

To identify and characterize the toxic forms of Aβ aggregates, we first examined *in vitro* aggregation conditions by using the chemically synthesized $Aβ_{1–40}$ and found that slow rotation of $Aβ_{1–40}$ solution reproducibly gave $Aβ_{1–40}$ aggregates containing a stable and highly neurotoxic moiety. Purification of the toxic moiety revealed that it is a perfect sphere, which we call amylospheroid (ASPD). Other moieties, including fibrils, were nontoxic. Second, we applied the above conditions to $Aβ_{1–42}$ and compared $Aβ_{1–42}$-ASPD with $Aβ_{1–40}$-ASPD. Finally, we used lithium to examine whether there is a link between ASPD toxicity and activation of glycogen synthase kinase-3β (GSK-3β) (18), which also is known as tau protein kinase I (TPKI) (19). Here, we describe the identification and characterization of ASPD and discuss its potential involvement in AD.

Materials and Methods

Synthesis of Aβs. $Aβ_{1–40}$ and $Aβ_{16–20}$ were synthesized and purified in Mitsubishi Kagaku Institute of Life Sciences by solid-phase fluorenylmethoxycarbonyl chemistry (>50% yield). Amino acid analysis, analytical HPLC, and matrix-assisted laser desorption ionization–time-of-flight mass spectrometry confirmed the purity of the products. The purified Aβs were lyophilized, dissolved in 35% CH_3CN in 0.1% trifluoroacetic acid, distributed into Eppendorf tubes (0.1 μmol), lyophilized, and kept at −20°C until used.

Preparation of Toxic $Aβ_{1–40}$ Aggregates by Slowly Rotating $Aβ_{1–40}$ Solution. $Aβ_{1–40}$ was synthesized or purchased from Bachem or U.S. Peptide (Rancho Cucamonga, CA). Toxic $Aβ_{1–40}$ aggregates were prepared as follows: $Aβ_{1–40}$ was suspended in 0.22-μm-filtered Milli Q water (700 μM), incubated at 4°C for 30 min, and diluted with 0.22-μm-filtered Dulbecco's PBS without Ca^{2+} and Mg^{2+} (PBS) (Nacalai Tesque, Kyoto) to 350 μM. $Aβ_{1–40}$ solution (350 μM) was rotated slowly at 37°C for 5–7 days by using a rotating cultivator. We describe toxic $Aβ_{1–40}$ aggregates prepared by slowly rotating $Aβ_{1–40}$ solution (350 μM in 50% PBS) as SR_{350}-$Aβ_{1–40}$. In some experiments, the concentration of $Aβ_{1–40}$ was reduced to 1 or 50 μM, which we describe as SR_1-$Aβ_{1–40}$ and SR_{50}-$Aβ_{1–40}$, respectively. In experiments using

This paper was submitted directly (Track II) to the PNAS office.

Abbreviations: Aβ, β-amyloid; AD, Alzheimer's disease; ADDL, Aβ-derived diffusible ligand; PF, protofibril; ASPD, amylospheroid; GSK-3β, glycogen synthase kinase-3β; TPKI, tau protein kinase I; SR-$Aβ_{1–40}$, slowly rotated $Aβ_{1–40}$ solution containing $Aβ_{1–40}$ aggregates; MTT, 3-(4,5-dimethylthiazol-2-yl)-2,5-diphenyltetrazolium bromide.

‡To whom correspondence should be addressed. E-mail: mie@libra.ls.m-kagaku.co.jp.

¶Present address: Fukuoka Women's University, 1-1-1 Kasumigaoka, Higashiku, Fukuoka 813-8529, Japan.

www.pnas.org/cgi/doi/10.1073/pnas.1237107100

$A\beta_{16-20}$ (KLVFF) (20) or $iA\beta5$ (LPFFD) (21) (Peptide Institute, Osaka), $A\beta_{1-40}$ solutions were mixed with a 10-fold molar excess of the pentapeptides at the onset of slow rotation.

Purification of ASPD from SR_{350}-$A\beta_{1-40}$. ASPD was isolated by eliminating fibrils from SR_{350}-$A\beta_{1-40}$ by filters with 0.65-μm and 30-kDa molecular sieves. For further purification, SR_{350}-$A\beta_{1-40}$ (0.11 ml) was centrifuged at 86,000 $\times$ *g* for 16 h (TLS55; Beckman Coulter) at 4°C in a 15–30% linear glycerol gradient. Ten-drop fractions were collected from the bottom. The pellet was suspended in 50% PBS (0.11 ml). Fractionated samples were examined immediately by immunoblotting, toxicity assays, and transmission electron microscopy. As a control, 50% PBS was centrifuged and analyzed similarly.

Preparation and Purification of $A\beta_{1-42}$-ASPD. Toxic $A\beta_{1-42}$ aggregates were prepared from $A\beta_{1-42}$ (Bachem) in essentially the same way as from $A\beta_{1-40}$, by slowly rotating $A\beta_{1-42}$ solutions (1–0.01 μM in 50% PBS) at 4°C for 8–10 h. $A\beta_{1-42}$-ASPD was purified from $SR_{0.1}$-$A\beta_{1-42}$ by using glycerol-gradient centrifugation as described above.

Transmission Electron Microscopy of ASPD. The isolated ASPD was negatively stained with 4% uranyl acetate solution on carbon-coated grids, analyzed immediately by JEOL JEM-1200EX/Top at 100 kV with an anticontamination system under liquid nitrogen, and photographed by using a minimum-dose system to prevent radiation damage. The size of ASPD was determined by NIH IMAGE or by measuring the diameter at the equator with a micrometer. Both methods gave similar results. In the case of unstained ASPD, ASPD was mixed with type VII agarose (1.0%; Sigma), fixed with 4% glutaraldehyde/PBS for 2 h, and embedded in Epon 812 resin (22). A horizontal thin section was made from the resin, and a cross section was made from a horizontal section, adjacent to the first one, reembedded in the resin. Both sections were examined by JEOL JEM-1230 at 100 kV.

Fluid-Phase Imaging of ASPD by Atomic Force Microscopy. The isolated ASPD was deposited on freshly cleaved mica (Nihon Veeco KK, Tokyo) that was modified with 3-aminopropylethoxysilane (23) and left for 30 min. Imaging was performed under 50% PBS by a multimode microscope with a Nanoscope III controller in a tapping-mode fluid cell (Digital Instruments, Santa Barbara, CA) by using A-scanner with 700-nm maximum lateral scan area. Silicon nitride probes coated with 0.5% polyethyleneimine (0.15 M borate buffer), attached to a 100-μm triangular cantilever (force constant of 0.08 N/m; Olympus, New Hyde Park, NY), were operated at 9-kHz resonant frequency with 0.5-Hz scan rates. Images were captured at 256 $\times$ 256 pixels.

Toxicity Assays. Primary cultures from rat septum regions, which include septal and basal forebrain cholinergic neurons, were prepared, and the medium (400 μl per well) was replaced with serum-free medium after 3 days *in vitro* (24). After 5 days *in vitro*, cultures were treated with either slowly rotated $A\beta_{1-40}$ solution (SR-Aβ) or ASPD. After a 16-h treatment, 3-(4,5-dimethylthiazol-2-yl)-2,5-diphenyl tetrazolium bromide (MTT) activity, a toxicity indicator (25, 26), was determined by measuring the absorbance at 570 nm. The background value was obtained by lysing cells with 0.1% Triton X-100 treatment for 10 min. Toxicity was estimated as inhibition of MTT activity compared with the control value obtained upon vehicle addition. After a 40-h treatment, cultures were rinsed and exposed for 30 min to propidium iodide (5 μM) and calcein-AM (0.2 μM) in 20 mM Hepes (pH 7.3) containing 130 mM NaCl, 5.4 mM KCl, 5.5 mM glucose, and 2 mM $CaCl_2$ at 37°C. Dye uptake was measured by using Zeiss Axiovert 200M with CoolSNAP HQ (Roper Scientific, Trenton, NJ) and analyzed with MetaMorph (Molecular Devices). Cells with shrunken or fragmented nuclear staining were counted as dead cells. The total cell number was assessed by Hoechst 33258 (1 μg/ml) staining after 10% formalin fixation. At least 1,200 cells were selected randomly from four different fields. Apoptotic activity was expressed as the ratio of apoptotic cells to the total cell number.

TPKI/GSK-3β Kinase Activity. Cultures were disrupted after the treatment, and TPKI/GSK-3β activity was determined (24).

Immunoblotting. Samples were separated on NOVEX 10–20% Tris/*N*-[tris(hydroxymethyl]glycine gels (Invitrogen). Immunoreactive bands with 4G8 (1 μg/ml; Signet Laboratories, Dedham, MA) were detected (27) by using SuperSignal West Femto substrates (Pierce).

Statistics. We examined the statistical significance of differences between groups by applying Games–Howell post hoc tests, using STATVIEW 5.0 (SAS Institute, Cary, NC).

Results

Preparation and Identification of Spherical $A\beta_{1-40}$ Aggregates (ASPD) as a Highly Toxic Moiety Among $A\beta_{1-40}$ Aggregates. We chemically synthesized $A\beta_{1-40}$ to obtain large quantities of homogenous peptide as starting material. After purification and characterization, $A\beta_{1-40}$ dissolved in 50% PBS to 350 μM was allowed to self-aggregate under various conditions, and the toxicity of each $A\beta_{1-40}$ solution was estimated by MTT activity by using primary cultures from rat septum regions. Initially, $A\beta_{1-40}$ solutions were nontoxic. When $A\beta_{1-40}$ solutions (Fig. 1*A*) were rotated slowly for 5–7 days, they showed potent toxicity at 0.1 μM. Without slow rotation, $A\beta_{1-40}$ solution remained nontoxic even at 5 μM (Fig. 1*A*). Therefore, we prepared toxic $A\beta_{1-40}$ aggregates by slowly rotating $A\beta_{1-40}$ solutions (350 μM in 50% PBS); the aggregates thus prepared are designated as SR_{350}-$A\beta_{1-40}$.

To identify the toxic moiety in SR_{350}-$A\beta_{1-40}$, we examined the structure–toxicity relationship of $A\beta_{1-40}$ aggregates during the course of slow rotation. $A\beta_{1-40}$ aggregates first detected by transmission electron microscopy consisted of spherical structures 3–20 nm in diameter without any detectable fibrils (Fig. 1*B*, 4 h). At 27 h, short, straight fibers and PF-like structures were detected, which disappeared when 6- to 10-nm-wide fibrils were formed at 75 h, whereas spherical structures continued to exist (Fig. 1*B*). MTT assay indicates that the toxicity of SR_{350}-$A\beta_{1-40}$ reached a plateau after 4 h of slow rotation, when spherical structures, but not fibrils, were present.

Next, $A\beta_{1-40}$ solutions at 350 μM (SR_{350}-$A\beta_{1-40}$), 50 μM (SR_{50}-$A\beta_{1-40}$), and 1 μM (SR_1-$A\beta_{1-40}$) each were rotated slowly for 7 days. Below a critical concentration ($\approx$100 μM) (28), the fibril formation in each SR-$A\beta_{1-40}$ was reduced drastically (Fig. 1*C Right*). However, with a decrease in the proportion of fibrils to other $A\beta_{1-40}$ aggregates in SR-$A\beta_{1-40}$, toxicity became much stronger (Fig. 1*C Left*), as shown by a decrease in IC_{50} (0.2 μM in SR_{350}-$A\beta_{1-40}$, 0.01 μM in SR_{50}-$A\beta_{1-40}$, and 0.001 μM in SR_1-$A\beta_{1-40}$). The kinetic studies further support a lack of toxicity in fibrils.

We inhibited the fibril formation by pentapeptides containing the $A\beta_{16-20}$ motif, which break β-sheet interactions required for the fibril formation. As reported previously, addition of $A\beta_{16-20}$ (KLVFF) (20) or $iA\beta_5$ (LPFFD) (21) at the onset of slow rotation led to $\approx$70% reduction in fibrils in SR_{350}-$A\beta_{1-40}$ in thioflavine T assay. However, toxicity of SR_{350}-$A\beta_{1-40}$ was unchanged (Fig. 1*D*). Slow rotation of the pentapeptides alone did not yield any toxicity. These results (Fig. 1 *B–D*) strongly suggest that $A\beta_{1-40}$ aggregates other than fibrils are responsible for the toxicity in SR-$A\beta_{1-40}$. We obtained similar results by using $A\beta_{1-40}$ from Bachem or U.S. Peptide.

In contrast to the fibril, the spherical structure (Fig. 1*B*, 4 h)

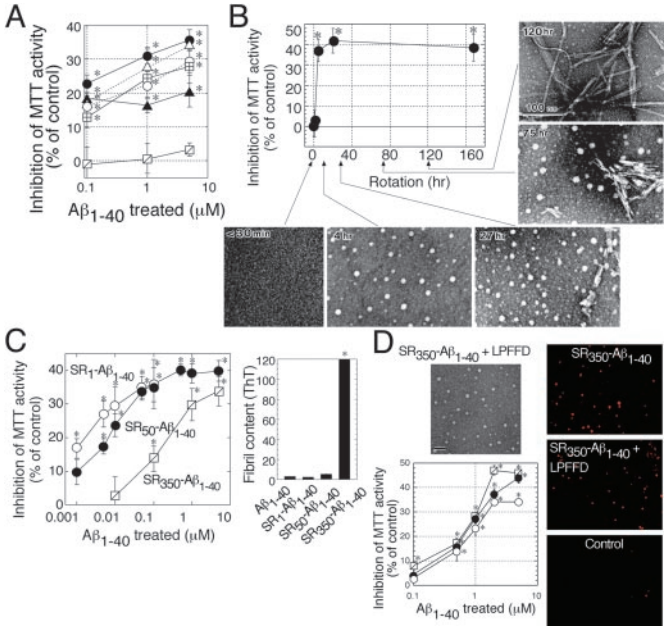

Fig. 1. ASPD as a neurotoxin in Aβ_{1-40} aggregates. (*A*) Aβ_{1-40} solutions (350 μM) were aggregated, and their toxicity was estimated by MTT assay ($n = 6$). Aβ_{1-40} solution was rotated in Eppendorf tubes (●), glass tubes (△), carbon-coated tubes (○), gold-coated tubes (⊞), and silicon-coated tubes (▲). Aβ_{1-40} solution without rotation also is shown (◪). Hereafter, we designated toxic Aβ_{1-40} aggregates formed by slowly rotating Aβ_{1-40} solution (350 μM in 50% PBS) as SR$_{350}$-Aβ_{1-40}. (*B*) The structure and toxicity of Aβ_{1-40} aggregates formed by slow rotation. At the indicated time, aliquots were removed from SR$_{350}$-Aβ_{1-40} for transmission electron microscopy and MTT assay ($n = 9$) (5 μM). (*C*) Aβ_{1-40} solutions [350 μM (SR$_{350}$-Aβ_{1-40}), 50 μM (SR$_{50}$-Aβ_{1-40}), and 1 μM (SR$_1$-Aβ_{1-40})] each were rotated slowly for 7 days, and the toxicity was assessed ($n = 7$). Thioflavine T assay (20 μM; Sigma; excitation at 445 nm and emission at 485 nm; ref. 48) determined fibril content in freshly dissolved Aβ_{1-40} and in each SR-Aβ_{1-40} ($n = 6$). (*D*) SR$_{350}$-Aβ_{1-40} was prepared with or without KLVFF or LPFFD. The toxicity was determined by MTT assay ($n = 9$) or propidium iodide staining (*Right*). Image of SR$_{350}$-Aβ_{1-40} with LPFFD is shown (bar, 100 nm). Also shown are SR$_{350}$-Aβ_{1-40} (○) with KLVFF (●) and with LPFFD (◪). Data represent the mean ± SE. *, Significant difference from the control. The results suggest that toxicity of SR$_{350}$-Aβ_{1-40} is associated with the spherical structures (*B*, 4 h), which we call ASPD.

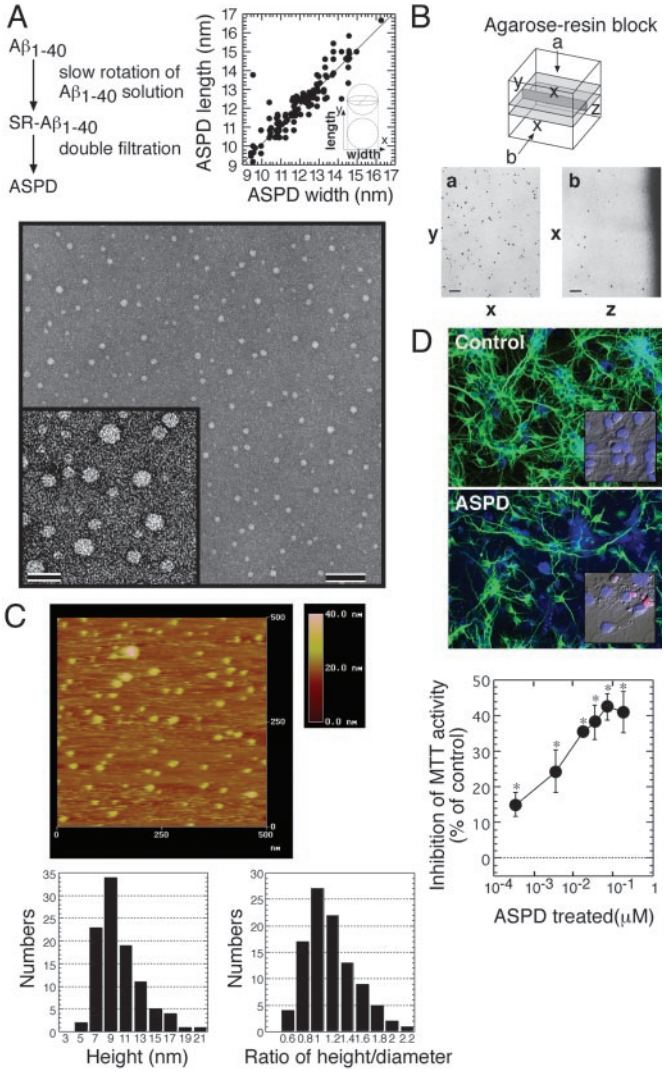

Fig. 2. ASPD morphology and toxicity. (*A*) Transmission electron microscopic images of isolated ASPD (bars, 100 nm in *Lower* and 20 nm in *Inset*). The width (x) and length (y) of each ASPD ($n = 101$) were measured (*Upper*). (*B*) Images of horizontal sections (*a*) and cross sections (*b*) of ASPD in the resin as described in *Materials and Methods*. (*C*) Fluid-phase atomic force microscopy of ASPD as described in *Materials and Methods* ($n = 100$). (*D*) Toxicity of ASPD. (*Top* and *Middle*) After a 40-h ASPD treatment (210 nM), cultures were stained with anti-MAP2 (green) and fillipin (blue). ASPD killed ≈40% neurons, with shrunken or fragmented nuclei stained pink with propidium iodide and Hoechst 33258 (*Inset*). Cell death in the control culture was <3%. (*Bottom*) ASPD toxicity was estimated by MTT activity ($n = 6$). Data in *D* represent the mean ± SE. *, Significant difference compared with control.

was not affected by the pentapeptides (Fig. 1*D*) and was present in SR-Aβ_{1-40} even under conditions in which fibrils were rarely detected owing to low Aβ_{1-40} concentrations. These results suggest that the spherical structure is the toxic moiety in SR-Aβ_{1-40}. In the following text, this spherical structure, a candidate neurotoxin in SR-Aβ_{1-40}, is designated as ASPD.

Morphology and Neurotoxicity of ASPD Isolated from SR-Aβ_{1-40}. ASPD was isolated in the flowthrough fraction of filters with 0.65-μM and 30-kDa molecular sieves, which contained only ASPD ranging from 4 to 18 nm (10.4 ± 2.9 nm on average, $n = 101$) with no fibrils (Fig. 2*A*). Based on measurement of the "width" and "length" of each ASPD in Fig. 2*A*, simple regression analysis was performed: $y/x = 0.982$, $r^2 = 0.869$, Δmean (width − length) = −0.1628 and $\Delta\sigma$ (width − length) = 0.7. These values support that ASPD is perfectly spherical. ASPD in the resin also gave circular images in both horizontal and cross sections (Fig. 2*B*), suggesting that ASPD is indeed a sphere.

To avoid possible effects of sample drying, which was necessary for transmission electron microscopy, the isolated ASPD was visualized in 50% PBS by atomic force microscopy. The shape of the section curve is consistent with a spherical shape of ASPD (Fig. 2*C*). Furthermore, a statistical analysis was carried out. In atomic force microscopy, the height is obtained precisely, whereas the length or the width is larger than the real value owing to effects depending on the radius of the probe. The radius of the probe (R) used here was estimated to be ≈2.5 nm (data not shown). If the sample is a sphere, its diameter ($2r$) can be calculated from the measured half-width (D) by using the following equation: $2r = -2R + 2\sqrt{R^2 + D^2}/4$. We measured the height and the half-width of each ASPD and obtained the height/calculated diameter ratio of each ASPD, which was 1.0 on average ($n = 100$) (Fig. 2*C*). These results confirmed that ASPD is a sphere, not a disk or a cylinder.

A 40-h treatment of neuronal cultures with the isolated ASPD (210 nM in Aβ_{1-40} monomer concentration) resulted in ≈40% neurodegeneration, with the remaining neurons displaying dis-

integrated neurites (Fig. 2*D Top* and *Middle*). Shrinkage and fragmentation of nuclei in ASPD-treated neurons stained with propidium iodide and Hoechst 33258 (Fig. 2*D Top* and *Middle Insets*) indicated apoptotic degeneration, whereas control cultures retained intact round nuclei. At all concentrations tested (0.35 nM to 0.175 μM; Fig. 2*D Bottom*), the isolated ASPD caused statistically significant inhibition of MTT activity (Games–Howell post hoc tests, $n = 6$). The isolated ASPD was stable over 2 months at 4°C and did not change to fibrils during another 7-day slow rotation. These results suggest that ASPD directly induced neurodegeneration.

Purification of the Toxic ASPD by Using Glycerol-Gradient Centrifugation. We purified ASPD further as in Fig. 3*A* by centrifugation (86,000 × *g*, 16 h) of SR_{350}-Aβ_{1-40} in a 15–30% linear glycerol gradient. Immediately after the centrifugation, the apoptotic activity and the Aβ content of each fraction were evaluated, and the specific cell death activity in Fig. 3*B* was calculated from these values that were obtained in four independent experiments.

We found that ASPD was distributed into two groups: toxic ASPD recovered in the bottom-most part of the gradient and nontoxic ASPD recovered in the upper part of the gradient (Fig. 3*B*). In repeated experiments, ASPD with the highest toxicity was found reproducibly in fraction 2 around the migration position of thyroglobulin (669 kDa). The toxic ASPD induced apoptosis in neuronal cultures after a 40-h treatment, whereas nontoxic ASPD in fraction 11 did not (Fig. 3*B Inset*). ASPD in fraction 2 showed an ≈450-fold-higher toxicity than fibrils and an ≈80-fold-higher toxicity than SR_{350}-Aβ_{1-40} (Fig. 3*B*).

Using ASPD purified by the glycerol gradient, we examined whether a correlation exists between the size of ASPD and its toxicity. The particle analysis of each fraction (Fig. 3*C*) clearly indicates that toxic ASPD consisted of particles >10 nm in transmission electron microscopy and nontoxic ASPD consisted of those <10 nm. ASPD in fraction 3 was <15 nm but exhibited toxicity equal to that of ASPD in fraction 1 (Fig. 3 *B* and *C*). Toxicity was absent in the flowthrough fraction of a filter with a 5-kDa molecular sieve size, suggesting a minor contribution to the toxicity from monomer or small oligomers that cannot be detected in transmission electron microscopy. Although there is still a possibility that species present in amounts too small to detect are involved, these results taken together indicate that potent toxicity is correlated best with 10- to 15-nm ASPD.

The toxic ASPD and nontoxic ASPD differed not only in apparent particle size but also in their band pattern in immunoblotting. As in Fig. 3*B*, at the onset of slow rotation, Aβ_{1-40} freshly dissolved in 50% PBS gave only a monomeric band, eluting as a single peak at a retention time corresponding to Aβ_{1-40} dimer in size-exclusion chromatography by using a Superdex 75 column (refs. 12, 17, and 29 and data not shown). After a 7-day slow rotation, SDS-stable oligomeric bands up to tetramers appeared in SR_{350}-Aβ_{1-40} (Fig. 3*B*, arrowheads), suggesting a change in the nature of Aβ_{1-40}. After glycerol-gradient centrifugation, the toxic ASPD in fractions 1–3 contained these SDS-stable oligomeric bands, but nontoxic ASPD did not (Fig. 3*B Upper*).

We applied the conditions established for Aβ_{1-40} to longer, more hydrophobic Aβ_{1-42}, which generally is considered to be more pathogenic than Aβ_{1-40}. Toxic Aβ_{1-42} aggregates were prepared by slowly rotating Aβ_{1-42} solutions (1–0.01 μM in 50% PBS) and were fractionated by using glycerol-gradient centrifugation. ASPD-like spheres with 3- to 20-nm diameters were detected after at least an 8-h slow rotation (Fig. 3*D Left*); they killed neurons at ≈0.35 nM (40-h treatment). In repeated fractionations, the highest toxicity was recovered reproducibly in fraction 2 ($n = 7$), ≈70% of which was accounted for by 10- to 14-nm ASPD-like spheres as shown by particle analysis (Fig. 3*D Right*). The specific cell death activity of Aβ_{1-42}-ASPD in fraction 2 was estimated to be at least ≈100-fold higher than that of Aβ_{1-40}-ASPD in fraction 2. In the case of Aβ_{1-40}, formation

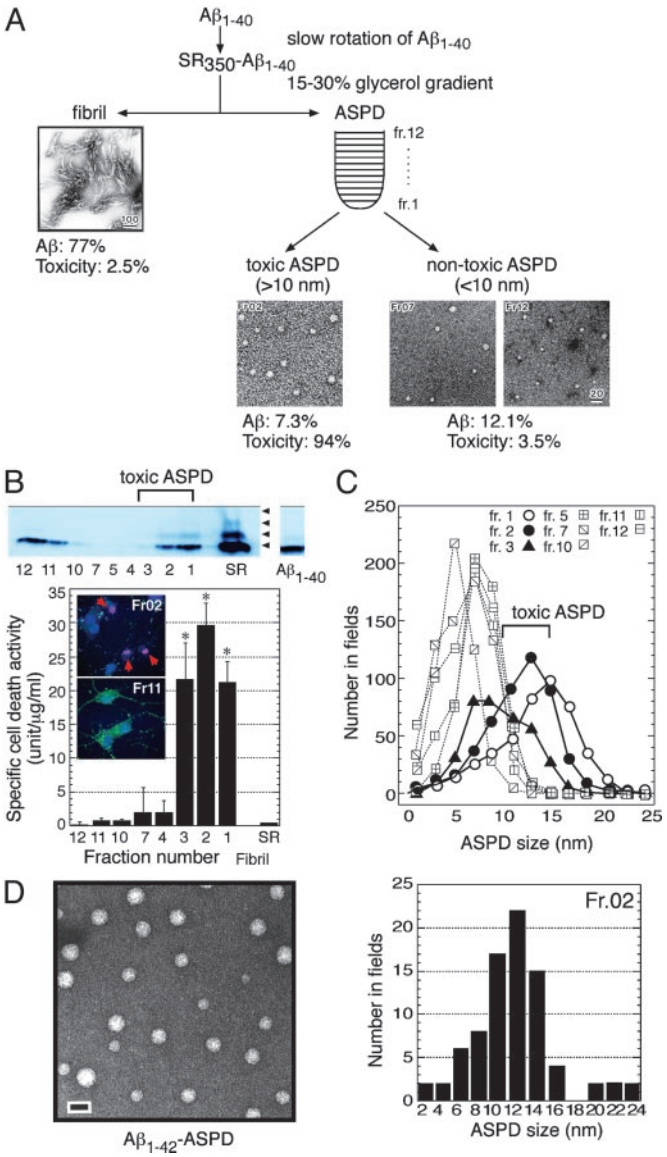

Fig. 3. Purification of toxic ASPD by the glycerol gradient. (*A*) ASPD and fibrils in SR_{350}-Aβ_{1-40} were fractionated as shown. Transmission electron microscopic images of representative fractions are shown. Aβ recovery and percentage of the total toxicity in glycerol gradient are indicated. (*B*) Immunoblottings with 4G8 of each fraction and of freshly dissolved Aβ_{1-40} are shown (*Upper*). Fraction 2 induced apoptotic cell death as shown by red arrows in propidium iodide and Hoechst 33258 staining, whereas fraction 11 did not (*Lower Inset*). Mini-Bradford assay quantitated Aβ content, using freshly dissolved Aβ_{1-40} as a standard, the concentration of which was determined accurately in advance with a Waters AccQTag system. Comparison of results from mini-Bradford assay with the AccQTag system data by using unfractionated SR_{350}-Aβ_{1-40} proved a good correlation at concentrations >1 μM. The specific cell death activity was calculated from the Aβ content and the apoptotic activity ($n = 16$); one unit is defined as the activity inducing 1% apoptotic cell death. The specific cell death activity values of unfractionated SR_{350}-Aβ_{1-40} and fibrils were 0.37 ± 0.09 and 0.07 ± 0.003, respectively. Data represent the mean ± SE. *, Significant difference compared with control. (*C*) The particle distribution of each fraction. (*D Left*) Transmission electron microscopic images of ASPD formed in Aβ_{1-42} solution (0.1 μM in 50% PBS) after an 8-h slow rotation (bar, 20 nm). (*Right*) Aβ_{1-42}-ASPD was separated by a glycerol gradient as in *A*. The particle distribution of fraction 2, in which the highest toxicity was recovered in repeated experiments ($n = 7$), is shown.

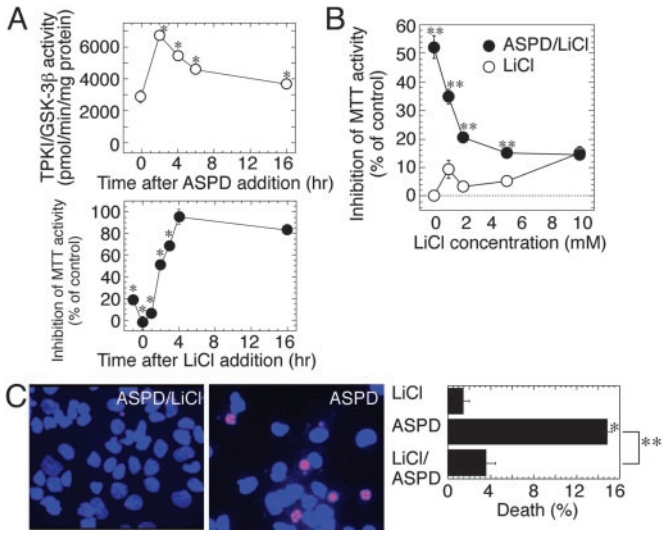

Fig. 4. Lithium suppression of ASPD toxicity. (*A Upper*) After 210-nM ASPD treatment, TPKI/GSK-3β activity was assayed at the indicated time (n = 6). (*Lower*) Lithium (2 mM) was added to ASPD-treated culture at the indicated time, and the toxicity was assayed (n = 6). (*B*) Dose-dependent inhibition of ASPD toxicity by lithium. Effect of lithium on 210-nM ASPD toxicity was examined (n = 6). (*C*) Lithium protection against ASPD-induced apoptosis. After the treatment, as indicated, propidium iodide and Hoechst 33258 staining was performed (n = 9). Data represent the mean ± SE. Significant difference compared with control (*) or with ASPD-treated culture (**).

of toxic ASPD requires a longer period of slow rotation with decrease in the initial concentration of Aβ_{1-40}: it took 4 h at 350 μM but >30 h at 50 μM. Aβ_{1-42} at lower concentrations formed ASPD much earlier than Aβ_{1-40}. These results demonstrated that Aβ_{1-42} forms ASPD, as Aβ_{1-40}, but Aβ_{1-42}-ASPD is formed more rapidly, induces neurodegeneration at lower concentrations, and is more toxic than Aβ_{1-40}-ASPD.

Toxicity of ASPD May Involve TPKI/GSK-3β Activation. We found a rapid increase in TPKI/GSK-3β activity in ASPD-treated neuronal cultures, which reached its maximum (≈2.8-fold) after a 2-h treatment, followed by a decline to a level 50% higher than that of the control (Fig. 4*A Upper*). TPKI/GSK-3β plays a crucial role in Aβ-triggered neuropathological cascades (19, 24, 30). Lithium has been suggested recently as a possible therapeutic reagent for AD, because of its ability to inhibit TPKI/GSK-3β activity (31, 32). Thus, we examined whether inhibition of TPKI/GSK-3β by lithium protects neurons against ASPD toxicity. Lithium suppressed the ASPD toxicity in a dose-dependent manner with an IC_{50} of ≈2 mM (Fig. 4*B*), which is similar to the reported IC_{50} of lithium on TPKI/GSK-3β activity (33). The addition of 2 mM lithium within 1 h after ASPD treatment protected cells against ASPD toxicity but had no effect 4 h after ASPD treatment (Fig. 4*A Lower*). Protective effects of lithium were confirmed further by using propidium iodide and Hoechst 33258 staining; in the presence of 2 mM lithium, apoptotic cell death induced by 210 nM ASPD was decreased significantly, nearly to the control level (Fig. 4*C*). These findings raise the possibility that TPKI/GSK-3β is involved in the early stages of the ASPD-induced neurodegenerative cascades.

Discussion

It is generally accepted that amyloids play a crucial role in neurodegenerative diseases such as AD. Nevertheless, the physiological function of Aβs has not been elucidated. There are several reasons for this. For example, Aβs in the *in vivo* state are not homogeneous but are mixtures of peptides with different sizes. Although Aβ_{1-40} is predominant among them (34), accumulated data have indicated that Aβ_{1-42} is the strongest candidate for the neurotoxic agent. In addition, the aggregation states of these peptides are controversial. Some reports suggest that fibrils are toxic, but others support dimer or oligomer as the real neurotoxin (reviewed in ref. 35). To avoid such ambiguities, we chemically synthesized large amounts of homogeneous Aβ_{1-40}. Although the solution of this preparation was not toxic, we found by chance that slow rotation of Aβ_{1-40} solution for 5–7 days converted Aβ_{1-40} to a stable form with potent toxicity (Fig. 1*B*). Purification and characterization of the toxic moiety provided evidence that a perfectly spherical Aβ_{1-40} aggregate is the most probable origin of the observed toxicity (Figs. 2 and 3). Other Aβ_{1-40} aggregates, including fibrils, were nontoxic. Therefore, we designated this toxic Aβ_{1-40} aggregate as ASPD. Correlation analysis in Fig. 3 indicated that toxicity is most closely associated with 10- to 15-nm ASPD, whereas ASPD <10 nm was nontoxic. We also found that Aβ_{1-42} forms ASPD, but Aβ_{1-42}-ASPD is formed more rapidly, induces neurodegeneration at a lower concentration (≈0.35 nM), and exhibits ≈100-fold-higher toxicity than Aβ_{1-40}-ASPD. Further analysis is required to elucidate the molecular basis of these differences. Because so far it is largely unknown how ASPD exerts its effect on neurons, we cannot completely rule out the possibility that very minor oligomers that have escaped detection are responsible for the toxicity. However, the data obtained up to the present support a positive correlation between the toxicity and ASPD >10 nm in the case of both Aβ_{1-40}-ASPD and Aβ_{1-42}-ASPD (Fig. 3) as well as when toxic ASPD in fraction 2 of the glycerol gradient was separated further by using size-exclusion chromatography (A.N., M.S., and M.H., unpublished data). Furthermore, the toxicity was not recovered in the flowthrough fraction of a filter with a 5-kDa molecular sieve size, suggesting that the toxicity is not attributable to monomer or small oligomers that cannot be detected in transmission electron microscopy.

PFs and ADDLs are two representative *in vitro* nonfibrillar neurotoxins detected by transmission electron microscopy or atomic force microscopy. Spherical ASPD is obviously different from curvilinear PFs (4- to 11-nm diameter and <200-nm length) (16, 17). ADDLs are a mixture of Aβ_{1-42} oligomers from trimers–hexamers up to 24-mers (15, 35). Because toxicity of ADDLs has been assessed in oligomer mixtures, it is difficult to know the precise size of the toxic moiety in ADDLs (15). The major component of ADDLs appeared to be globules of 4.8–5.7 nm in atomic force microscopy with 17- and 22-kDa bands in immunoblotting (15). We could not find any correlation between the toxicity and spheres of ≈5 nm derived from Aβ_{1-42} or Aβ_{1-40} in glycerol-gradient fractionation. ASPD showed an apparent size of 9.2 nm on average in atomic force microscopy and contained SDS-stable oligomeric bands up to tetramers. Formation of ADDLs seems to be restricted to Aβ_{1-42} when fibril formation is suppressed (15), whereas ASPD is formed from either Aβ_{1-40} or Aβ_{1-42} irrespective of fibril formation. Thus, ASPD differs from ADDLs in size, the band composition in immunoblotting, and preparation method. Under the conditions examined, Aβ remained nontoxic without slow rotation (Fig. 1*A*). Slow rotation has been reported to enhance the aggregation of yeast prion (36) or hemoglobin S (37). Because ASPD is formed below the concentration required for fibril formation and in the presence of β-sheet-breaking peptides (Fig. 1 *C* and *D*), Aβ may aggregate into ASPD, at least in part, through a distinct pathway from fibril formation. Thus, it is possible that slow rotation of Aβ solution leads to some as-yet-unknown structural changes in Aβ that induce spherical aggregation, because SDS-stable oligomeric bands of Aβ_{1-40} are seen only in toxic

ASPD. Further studies are required to understand the aggregation process of Aβ into ASPD and the relationship of ASPD with fibrils and other nonfibrillar oligomers.

Recent *in vivo* as well as *in vitro* studies support the toxicity of nonfibrillar oligomers and their possible causative role in neuropathology in AD (8, 35, 38), which is consistent with the dissociation between fibril loads and the cognitive decline in AD (39–41). Because vaccination, in some cases, has protected transgenic mice from memory loss without a significant decrease in Aβ fibril loads (5), Aβ aggregates other than fibrils may be the preferred therapeutic targets for AD (35). However, the nature of Aβ species and the oligomer state responsible for the pathogenesis remain controversial owing to the heterogeneity of Aβ aggregates in terms of Aβ species and oligomer size. Fractionation studies using an *in vitro* Aβ aggregation system as shown here will help to elucidate the aggregation process and to determine the oligomerization state of Aβ causing the pathogenesis.

In AD brains, intracellular accumulation of nonfibrillar Aβ, especially $A\beta_{1-42}$ (42, 43), precedes the extracellular fibrillar accumulation of Aβ as senile plaques (1). Recently, LeBlanc *et al.* (44) have shown that microinjection of $A\beta_{1-42}$ kills neurons. In their experiments, extracellular treatment of neurons with $A\beta_{1-42}$ or $A\beta_{1-40}$ did not affect the viability, despite the reported toxicity. These findings indicate the biological significance of intracellular Aβ accumulation but, at the same time, also raise the question of the source of intracellular Aβ *in vivo* (44): how does Aβ, which is produced through the secretory pathway, enter the cytosol? In our preliminary experiments, SDS-resistant oligomeric bands could be detected by immunoblotting in cytosolic extracts of neuronal cultures within 1 h after extracellular ASPD treatment (M.H. and M.S., unpublished data). If Aβ really exerts its effect intracellularly, variability in biological activities among *in vitro* identified Aβ aggregates may be attributed to their differing ability to access the cytosol. Future experiments to examine how ASPD enters the cytosol may provide some clue to the apparent contradiction between intracellular and extracellular Aβ accumulation.

Lithium, one of the most widely used drugs for bipolar disorder, protects neurons against suboptimal conditions or from excitotoxicity-induced lesions (reviewed in ref. 45). Here, we found that lithium may protect neurons in the early phase of ASPD treatment, perhaps through inhibition of TPKI/GSK-3β activation. Possible use of lithium as a therapeutic reagent for AD has been suggested by several authors (31–33, 46, 47). Considering the important role of TPKI/GSK-3β in AD, more detailed studies on the molecular mechanism of the lithium protection against ASPD may help to design inhibitors of TPKI/GSK-3β as candidate drugs for the treatment of AD.

We thank Dr. T. Wakabayashi for comments on ASPD structure; A. Ito, Y. Sakamoto, and C. Aoyama for technical assistance; and Drs. R. L. Veech, Y. Kashiwaya, and D. Masui for discussion. We are grateful to Dr. K. Imahori for critically reading the manuscript. M.H. was supported by a grant from Japan Science and Technology Corp. This work was supported by grants from Mitsubishi Kagaku Institute of Life Sciences, Japan Science and Technology Corp., and the Organization for Pharmaceutical Safety and Research.

1. Glenner, G. G. & Wong, C. W. (1984) *Biochem. Biophys. Res. Commun.* **120,** 885–890.
2. Selkoe, D. J. (2001) *Physiol. Rev.* **81,** 741–766.
3. Schenk, D., Barbour, R., Dunn, W., Gordon, G., Grajeda, H., Guido, T., Hu, K., Huang, J., Johnson-Wood, K., Khan, K., *et al.* (1999) *Nature* **400,** 173–177.
4. Janus, C., Pearson, J., McLaurin, J., Mathews, P. M., Jiang, Y., Schmidt, S. D., Chishti, M. A., Horne, P., Heslin, D., French, J., *et al.* (2000) *Nature* **408,** 979–982.
5. Morgan, D., Diamond, D. M., Gottschall, P. E., Ugen, K. E., Dickey, C., Hardy, J., Duff, K., Jantzen, P., DiCarlo, G., Wilcock, D., *et al.* (2000) *Nature* **408,** 982–985.
6. Levine, H., III (1995) *Neurobiol. Aging* **16,** 755–764.
7. Hartley, D. M., Walsh, D. M., Ye, C. P., Diehl, T., Vasquez, S., Vassilev, P. M., Teplow, D. B. & Selkoe, D. J. (1999) *J. Neurosci.* **19,** 8876–8884.
8. Walsh, D. M., Klyubin, I., Fadeeva, J. V., Cullen, W. K., Anwyl, R., Wolfe, M. S., Rowan, M. J. & Selkoe, D. J. (2002) *Nature* **416,** 535–539.
9. Pike, C. J., Burdick, D., Walencewicz, A. J., Glabe, C. G. & Cotman, C. W. (1993) *J. Neurosci.* **13,** 1676–1687.
10. Lorenzo, A. & Yankner, B. A. (1994) *Proc. Natl. Acad. Sci. USA* **91,** 12243–12247.
11. Hardy, J. A. & Higgins, G. A. (1992) *Science* **256,** 184–185.
12. Garzon-Rodriguez, W., Sepulveda-Becerra, M., Milton, S. & Glabe, C. G. (1997) *J. Biol. Chem.* **272,** 21037–21044.
13. Roher, A. E., Chaney, M. O., Kuo, Y. M., Webster, S. D., Stine, W. B., Haverkamp, L. J., Woods, A. S., Cotter, R. J., Tuohy, J. M., Krafft, G. A., *et al.* (1996) *J. Biol. Chem.* **271,** 20631–20635.
14. Gajewski, T. F., Fields, P. & Fitch, F. W. (1995) *Eur. J. Immunol.* **25,** 1836–1842.
15. Lambert, M. P., Barlow, A. K., Chromy, B. A., Edwards, C., Freed, R., Liosatos, M., Morgan, T. E., Rozovsky, I., Trommer, B., Viola, K. L., *et al.* (1998) *Proc. Natl. Acad. Sci. USA* **95,** 6448–6453.
16. Harper, J. D., Wong, S. S., Lieber, C. M. & Lansbury, P. T. (1997) *Chem. Biol.* **4,** 119–125.
17. Walsh, D. M., Lomakin, A., Benedek, G. B., Condron, M. M. & Teplow, D. B. (1997) *J. Biol. Chem.* **272,** 22364–22372.
18. Ali, A., Hoeflich, K. P. & Woodgett, J. R. (2001) *Chem. Rev.* **101,** 2527–2540.
19. Imahori, K. & Uchida, T. (1997) *J. Biochem. (Tokyo)* **121,** 179–188.
20. Tjernberg, L. O., Naslund, J., Lindqvist, F., Johansson, J., Karlstrom, A. R., Thyberg, J., Terenius, L. & Nordstedt, C. (1996) *J. Biol. Chem.* **271,** 8545–8548.
21. Soto, C., Sigurdsson, E. M., Morelli, L., Kumar, R. A., Castano, E. M. & Frangione, B. (1998) *Nat. Med.* **4,** 822–826.
22. Luft, J. H. (1961) *J. Biophys. Biochem. Cytol.* **9,** 409–414.
23. Lyubchenko, Y. L., Gall, A. A., Shlyakhtenko, L. S., Harrington, R. E., Jacobs, B. L., Oden, P. I. & Lindsay, S. M. (1992) *J. Biomol. Struct. Dyn.* **10,** 589–606.
24. Hoshi, M., Takashima, A., Noguchi, K., Murayama, M., Sato, M., Kondo, S., Saitoh, Y., Ishiguro, K., Hoshino, T. & Imahhori, K. (1996) *Proc. Natl. Acad. Sci. USA* **93,** 2719–2723.
25. Shearman, M. S., Ragan, C. I. & Iversen, L. L. (1994) *Proc. Natl. Acad. Sci. USA* **91,** 1470–1474.
26. Liu, Y. & Schubert, D. (1997) *J. Neurochem.* **69,** 2285–2293.
27. Ida, N., Hartmann, T., Pantel, J., Schroder, J., Zerfass, R., Forstl, H., Sandbrink, R., Masters, C. L. & Beyreuther, K. (1996) *J. Biol. Chem.* **271,** 22908–22914.
28. Lomakin, A., Chung, D. S., Benedek, G. B., Kirschner, D. A. & Teplow, D. B. (1996) *Proc. Natl. Acad. Sci. USA* **93,** 1125–1129.
29. Huang, T. H., Yang, D. S., Plaskos, N. P., Go, S., Yip, C. M., Fraser, P. E. & Chakrabartty, A. (2000) *J. Mol. Biol.* **297,** 73–87.
30. Takashima, A., Noguchi, K., Sato, K., Hoshino, T. & Imahori, K. (1993) *Proc. Natl. Acad. Sci. USA* **90,** 7789–7793.
31. Hong, M., Chen, D. C., Klein, P. S. & Lee, V. M. (1997) *J. Biol. Chem.* **272,** 25326–25332.
32. Sun, X., Sato, S., Murayama, O., Murayama, M., Park, J. M., Yamaguchi, H. & Takashima, A. (2002) *Neurosci. Lett.* **321,** 61–64.
33. Klein, P. S. & Melton, D. A. (1996) *Proc. Natl. Acad. Sci. USA* **93,** 8455–8459.
34. Shoji, M., Golde, T. E., Ghiso, J., Cheung, T. T., Estus, S., Shaffer, L. M., Cai, X.-D., McKay, D. M., Tintner, R., Frangione, B., *et al.* (1992) *Science* **258,** 126–129.
35. Klein, W. L., Krafft, G. A. & Finch, C. E. (2001) *Trends Neurosci.* **24,** 219–224.
36. DePace, A. H., Santoso, A., Hillner, P. & Weissman, J. S. (1998) *Cell* **93,** 1241–1252.
37. Briehl, R. W. (1980) *Nature* **288,** 622–624.
38. Bucciantini, M., Giannoni, E., Chiti, F., Baroni, F., Formigli, L., Zurdo, J., Taddei, N., Ramponi, G., Dobson, C. M. & Stefani, M. (2002) *Nature* **416,** 507–511.
39. Dickson, D. W. & Yen, S. H. (1989) *Neurobiol. Aging* **10,** 402–404, 412–414.
40. Terry, R. D., Masliah, E., Salmon, D. P., Butters, N., DeTeresa, R., Hill, R., Hansen, L. A. & Katzman, R. (1991) *Ann. Neurol.* **30,** 572–580.
41. Lue, L. F., Kuo, Y. M., Roher, A. E., Brachova, L., Shen, Y., Sue, L., Beach, T., Kurth, J. H., Rydel, R. E. & Rogers, J. (1999) *Am. J. Pathol.* **155,** 853–862.
42. Gouras, G. K., Tsai, J., Naslund, J., Vincent, B., Edgar, M., Checler, F., Greenfield, J. P., Haroutunian, V., Buxbaum, J. D., Xu, H., *et al.* (2000) *Am. J. Pathol.* **156,** 15–20.
43. D'Andrea, M. R., Nagele, R. G., Wang, H. Y., Peterson, P. A. & Lee, D. H. (2001) *Histopathology* **38,** 120–134.
44. Zhang, Y., McLaughlin, R., Goodyer, C. & LeBlanc, A. (2002) *J. Cell Biol.* **156,** 519–529.
45. Jope, R. S. (1999) *Mol. Psychiatry* **4,** 117–128.
46. Stambolic, V., Ruel, L. & Woodgett, J. R. (1996) *Curr. Biol.* **6,** 1664–1668.
47. Alvarez, G., Munoz-Montano, J. R., Satrustegui, J., Avila, J., Bogonez, E. & Diaz-Nido, J. (1999) *FEBS Lett.* **453,** 260–264.
48. LeVine, H., III (1993) *Protein Sci.* **2,** 404–410.